

On the use of the Discrete Variable Representation Basis in Nuclear Physics

Aurel Bulgac¹ and Michael McNeil Forbes^{1,2}

¹*Department of Physics, University of Washington, Seattle, Washington 98195-1560 USA and*

²*Institute for Nuclear Theory, University of Washington, Seattle, Washington 98195-1550 USA*

(Dated: Wednesday 31st August, 2022)

The discrete variable representation (DVR) basis is nearly optimal for numerically representing wave functions in nuclear physics: Suitable problems enjoy exponential convergence, yet the Hamiltonian remains sparse. We show that one can often use smaller basis sets than with the traditional harmonic oscillator basis, and still benefit from the simple analytic properties of the DVR bases which requires no overlap integrals, simply permit using various Jacobi coordinates, and admit straightforward analyses of the ultraviolet (UV) and infrared (IR) convergence properties.

PACS numbers: 21.60.-n, 21.10.-k, 03.65.Ge,

PROBLEMS in nuclear physics typically require solving the one-body Schrödinger equation in three-dimensions. Numerically representing wavefunctions requires limiting both ultraviolet (UV) and infrared (IR) scales: a finite spatial resolution (i.e., a lattice) characterizes the highest representable momenta Λ , while a finite size (i.e. a cubic box of volume L^3) determines the largest physical extent. Nuclear structure calculations are historically dominated by the use of the harmonic oscillator (HO) basis of HO wave functions. The appeal of the HO basis stems from the shape of the self-consistent field obtained for small nuclei, which can be approximated by a harmonic potential at small distances from the center of the nucleus. One can also use the Talmi-Moshinsky transformation to separate out the center-of-mass motion in products of single particle HO wavefunctions. Recent efforts have been made to determine a minimal HO basis set, and to understand its convergence and accuracy [1, 2].

Here we advocate that the discrete variable representation (DVR) – in particular the Fourier plane-wave basis – enjoy most of the advantages of the HO basis, but with a significant improvement in terms of computational efficiency and simplicity, thereby admitting straightforward UV and IR convergence analyses and implementation.

Consider wavefunctions in a cubic box of volume L^3 with momenta less than Λ . The total number of quantum states in such a representation is given by the following intuitive formula – the ratio of the total phase space volume to the phase space volume of a single 3D quantum state:

$$N_{\text{QS}} = \left(\frac{L 2\Lambda}{2\pi\hbar} \right)^3. \quad (1)$$

One obtains the same result [3] using Fourier analysis: there are exactly N_{QS} linearly independent functions in a cubic 3D box of volume L^3 with periodic boundary conditions and wave-vectors less than $k_c = \Lambda/\hbar$ in each direction. These can be conveniently represented in the coordinate representation with N equally spaced points in each direction and lattice constant $a = \pi/k_c = \pi\hbar/\Lambda =$

L/N for a total of $N^3 = N_{\text{QS}}$ coefficients. The maximum wave-vector k_c is simply the Nyquist frequency [3] – one gains nothing by sampling the functions on intervals (“times”) finer than a .

The wavefunctions can also be represented in momentum space using a discrete fast Fourier transform (FFT) [4]. The momentum representation consists of N_{QS} coefficients on a 3D cubic lattice with spacing $2\pi\hbar/L$ and extent $-\Lambda \leq p_{x,y,z} < \Lambda$. Using the FFT to calculate spatial derivatives is not only fast, but extremely accurate – often faster and more accurate than finite difference formulas. We use an even number of lattice points ($N = 2^n$ is best for the FFT) and quantize the three momenta ($p_{x,y,z} = \hbar k_{x,y,z}$)

$$p_k = \frac{2\pi k\hbar}{L}, \quad x_k = ak, \\ k \in \left(-\frac{N}{2}, -\frac{N}{2} + 1, \dots, \frac{N}{2} - 1 \right). \quad (2)$$

The Fourier basis uses plane waves – e.g. $\exp(ik_n x)$ in the x -direction – but these can be linearly combined to form an equivalent sinc-function basis:

$$\psi_k(x) = \text{sinc } k_c(x - x_k) = \frac{\sin k_c(x - x_k)}{k_c(x - x_k)}. \quad (3)$$

This is similar to the difference between Bloch and Wannier wave functions in condensed matter physics. An advantage of this basis is that it is quasi-local $\psi_k(x_l) = \delta_{kl}$ allowing one to represent external potentials as a diagonal matrix $V_{kl} \approx V(x_k)\delta_{kl}$ (19).

The plane wave basis can thus be interpreted as a periodic DVR basis set, which has been discussed extensively in literature (see [5–8] and the references therein), and one can take advantage of Fourier techniques and the useful DVR properties.

In general, DVR bases are characterized by two scales: a UV scale $\Lambda = \hbar k_c$ defining the largest momentum representable in the basis, and an IR scale L defining the maximum extent of the system. In many cases, the basis is constructed by projecting Dirac delta-functions onto the finite-momentum subspace: For example, the sinc-function basis (3) is precisely the set of projected

Dirac delta functions $\psi_n(x) = P_{p \leq \Lambda} \delta(\mathbf{r} - \mathbf{r}_\alpha)$ onto the subspace $|\mathbf{p}| \leq \Lambda$ [5–7]. (It can be non-trivial, however, to choose a consistent set of abscissa maintaining the quasi-locality property.) The basis thus optimally covers the region $[-L/2, L/2] \times [-\Lambda, \Lambda]$ for each axis in phase space, and leads to an efficient discretization scheme with exponential convergence properties.

The DVR basis admits a straightforward analysis of the UV and IR limits, allowing one to construct effective extrapolations to the continuum and thermodynamic limits respectively. The UV effects may be analyzed by simply considering the properties of the projection $P_{p \leq \Lambda}$ used to define the basis, and the IR limit for periodic basis is well understood by techniques like those derived by Beth, Uhlenbeck, and Lüscher [9, 10]. We would like to emphasize an additional technique here: The IR limit is characterized by $2\pi\hbar/L$ – the smallest interval in momentum space resolvable with the basis set. For some problems, one can efficiently circumvent this limitation by using “twisted” boundary conditions $\psi(\mathbf{r} + \mathbf{L}) = \exp(i\theta_B)\psi(\mathbf{r})$ or Bloch waves as they are known in condensed matter physics. In particular, averaging over $\theta_B \in [0, 2\pi)$ will completely remove any IR limitations (without changing the basis size) for periodic and homogeneous problems, effectively “filling-in” the momentum states $p_n \leq p_n + \hbar\theta_B/L < p_{n+1}$. Extensions of these formulas to the case of a box with unequal sides is straightforward.

To demonstrate the properties of the DVR basis, we contrast it with the HO basis. The periodic DVR basis (plane-waves) shares the ease of separating out the center-of-mass. In particular, one can use Jacobi coordinates to separate out the center-of-mass motion without evaluating Talmi-Moshinsky coefficients, leading to simpler and more transparent implementations. The quasi-locality of the DVR basis offers an additional implementation advantage over the HO basis: one need not compute wavefunction overlaps to form the potential energy matrix. In contrast with the HO basis, the kinetic energy matrix \mathbf{K} is no-longer diagonal, but it has an explicit formula (24), and is quite sparse, unlike the potential energy operator in the HO basis.

Consider the HO wavefunctions with energy $E \leq \hbar\omega(N + 3/2)$: the maximum radius and momenta are

$$R = \sqrt{2N + 3} b, \quad \Lambda = \sqrt{2N + 3} \frac{\hbar}{b}, \quad (4)$$

where $b = \sqrt{\hbar/m\omega}$ is the oscillator length. For large N , $N \approx R\Lambda/2\hbar$. Thus, to expand a wavefunction with extent $2R$ containing momenta $|\mathbf{p}| < \Lambda$ requires at least

$$N_{\text{HO}} = \frac{(N + 1)(N + 2)(N + 3)}{6} \approx \frac{1}{6} \left(\frac{R\Lambda}{2\hbar} \right)^3 \quad (5)$$

states. To contrast, the DVR basis covering the required volume of phase space (1) with $L = 2R$ and Λ is

$$N_{\text{DVR}} = \left(\frac{2R \Lambda}{2\pi\hbar} \right)^3. \quad (6)$$

The ratio in the limit $N \rightarrow \infty$ is thus

$$\frac{N_{\text{DVR}}}{N_{\text{HO}}} = \frac{384}{\pi^3} \approx 12.4. \quad (7)$$

Since these states are localized, one can further impose Dirichlet boundary conditions, allowing functions only of the type $\sin(k_n x)$ with $k_n L = n\pi$ (instead of $\exp(ik_n x)$), thereby keeping only half of the momenta:

$$\frac{N_{\text{DVR}}}{N_{\text{HO}}} = \frac{48}{\pi^3} \approx 1.5. \quad (8)$$

Choosing a cubic box with Dirichlet boundary conditions, sides $L = 40$ fm, and maximum momentum $\Lambda = 300$ MeV/c gives

$$N_{\text{DVR}} = \left(\frac{L \Lambda}{2\pi\hbar} \right)^3 \approx 10^3, \quad (9)$$

a somewhat surprisingly small number of states. For symmetric states, one could further reduce the basis by imposing cubic symmetry, decreasing the basis size by another factor of 8.

Finally, one can fully utilize spherical symmetry with a related Bessel-function DVR basis gaining a factor of $\pi/6$, and thereby besting the HO basis

$$\frac{N_{\text{DVR}}}{N_{\text{HO}}} = \frac{8}{\pi^2} \approx 0.8 < 1. \quad (10)$$

In this counting, spin and isospin degrees of freedom which occur in both bases have been omitted.

The Bessel-function DVR basis set [5–7, 11] follows from a similar procedure of projecting Dirac delta functions for the radial Schrödinger equation. The angular coordinates are treated in the usual manner using spherical harmonics, but the radial wavefunctions are based on the Bessel functions (see Refs. [7, 11] for details) which satisfy the orthogonality conditions

$$\int_0^{k_c} dk \frac{2k}{k_c^2} \frac{J_\nu(kr_{v\alpha})J_\beta(kr_{v\beta})}{|J'_\nu(kr_{v\alpha})J'_\beta(kr_{v\beta})|} = \delta_{\alpha\beta}, \quad (11)$$

where $z_{v\alpha} = k_c r_{v\alpha}$ – the zeros of the Bessel functions $J_\nu(z_{v\alpha}) = 0$ – define the radial abscissa $r_{v,\alpha}$. The DVR basis set is

$$F_{\nu n}(r) = \sqrt{r} J_\nu \left(\frac{z_{\nu n} r}{R} \right), \quad z_{\nu n} = k_c r_{\nu n}. \quad (12)$$

Integral and differential operators have simple forms in the DVR basis (see Refs. [5–7] and the code [12, 13]). In principle, a different basis (and corresponding abscissa) should be used for each angular momentum quantum number ν ; In practice, good numerical accuracy is obtained using the $\nu = 0$ basis $j_0(z_{0n} r/R)$ and the $\nu = 1$ basis $j_1(z_{1n} r/R)$ respectively for even and odd partial waves [11, 12]. In the s -waves case, the abscissa

are simply the zeros of the spherical Bessel function $j_0(z) = \sin(z)/z$:

$$z_{0n} = n\pi, \quad r_{0n} = \frac{n\pi}{k_c}, \quad n = 1, 2, 3, \dots, N, \quad (13)$$

and correspond to the 1D basis with Dirichlet boundary conditions mentioned earlier. The zeros for $j_1(z)$ lie between the zeros of $j_0(z)$. The number of DVR functions needed to represent with exponential accuracy a radial wavefunction is

$$\mathcal{N}_{0\text{DVR}} = \frac{Rk_c}{\pi}, \quad (14)$$

to be compared (in the limit $N \rightarrow \infty$) with

$$\mathcal{N}_{0\text{HO}} = \frac{Rk_c}{4}. \quad (15)$$

In the last formula we have divided by an additional factor of 2, since $N = 2n + 1$ changes in steps of 2.

A major drawback of the HO wavefunctions that is rarely mentioned is that, for modest values of N and $l \neq 0$, the radial wave functions concentrate in two distinct regions: around the inner and outer turning points of the effective potential $V(r) = \hbar^2 l(l+1)/2mr^2 + m\omega^2 r^2/2$. By adding components with larger values of N , one modifies the wavefunction at both small and large distances, leading to slow convergence. In contrast, the DVR functions are concentrated around a single lattice site. Thus, adding more components only affects the solution in the vicinity of the additional lattice points leaving the states largely unaffected elsewhere.

For nuclei one can gain insight with some estimates. Cutoffs of $\Lambda = 600 \text{ MeV}/c$ and $R = 1.5 \dots 2A^{1/3} \text{ fm}$ should satisfy most of the practical requirements, leading to

$$b = \sqrt{\frac{\hbar R}{\Lambda}} \approx 0.7 \dots 0.8 A^{1/6} \text{ fm}, \quad (16a)$$

$$\hbar\omega = \frac{\hbar^2}{mb^2} = \frac{\hbar\Lambda}{mR} \approx 60 \dots 80 A^{-1/3} \text{ MeV}, \quad (16b)$$

compared to the value $40 A^{-1/3} \text{ MeV}$ one finds in typical monographs [14]. Using only half the value of $\Lambda = 300 \text{ MeV}/c$ naturally halves the value of $\hbar\omega$.

We end with demonstrations of the DVR method [13]. We start with the harmonic oscillator problem in 1D

$$H\phi(x) = \left(-\frac{\hbar^2}{2m} \frac{d^2}{dx^2} + \frac{k_c^2 x^2}{2R^2} \right) \phi(x) = E\phi(x), \quad (17)$$

where we choose the harmonic oscillator frequency according to Eq. (16b), varying the lattice constant $a = \pi/k_c$ and $L = Na$. The DVR method is sometimes referred to as the Lagrange method in numerical analysis [8], and functions are usually represented on the spatial lattice

$$\psi(x) = \sum_k \alpha \psi(x_k) f_k(x), \quad \langle f_k | f_l \rangle = \delta_{kl}. \quad (18)$$

Potential matrix elements usually have a simple and unexpectedly accurate representation (quasi-locality)

$$\langle f_k | V | f_l \rangle = \int dx f_k^*(x) V(x) f_l(x) \approx V(x_k) \delta_{kl}, \quad (19)$$

where the functions $f_k(x)$ are a linear combination of plane-waves and form an orthonormal set (these formulae apply for even numbers of abscissa as required by efficient implementations of the FFT)

$$f_k(x_l) = \sum_{n=-N/2}^{N/2-1} \frac{1}{L} \exp \frac{ip_n(x_l - x_k)}{\hbar} = \begin{cases} \frac{\sin \pi(k-l)}{Na} \cotan \frac{\pi(k-l)}{N} = 0 & k \neq l, \\ 1/a & k = l, \end{cases} \quad (20)$$

$$\psi(x_k) = \sum_l \alpha f_k(x_l) \psi(x_l), \quad (21)$$

where x_k and p_n were defined in Eq. (2). As before, the functions $f_k(x_l)$ are simply the normalized projections of the periodic Dirac functions on the DVR subspace [5–7], and satisfy

$$\sum_n \alpha f_k(x_n) f_l(x_n) = \delta_{kl}. \quad (22)$$

The sinc-function basis (3) is obtained in the limit $N \rightarrow \infty$ (if $a = 1$). Derivatives can be computed using the projected derivative of the Dirac delta function $g_x(x)$,

$$g_k(x_l) = \frac{(-1)^{l-k}}{Na^2} \cotan \frac{\pi(l-k)}{N} (1 - \delta_{kl}), \quad (23a)$$

$$\left. \frac{d\psi(x)}{dx} \right|_{x=x_k} = \sum_l \alpha g_k(x_l) \psi(x_l) \quad (23b)$$

and is exact for all momenta except for the highest one $p_{\text{max}} = \hbar\pi/a$. Some care must be taken when dealing with this state, but physics should not depend on this if Λ is properly chosen.

While the potential matrix is diagonal, the DVR kinetic energy is a matrix in coordinate representation:

$$K_{kl} = \begin{cases} \frac{\hbar^2 \pi^2}{mN^2 a^2} \frac{(-1)^{k-l}}{\sin^2 \frac{\pi(k-l)}{N}} & k \neq l \\ \frac{\hbar^2 \pi^2}{6m a^2} \left(1 + \frac{2}{N^2} \right) & k = l. \end{cases} \quad (24)$$

This matrix is full matrix in 1D, but sparse in 3D where only $1/N^2$ of the matrix elements are non-vanishing. The HO Hamiltonian (17) is thus represented in the DVR basis with periodic boundary conditions as

$$H_{kl} = K_{kl} + \frac{m\omega^2 a^2 k^2}{2} \delta_{kl}. \quad (25)$$

The implementation of Dirichlet boundary conditions uses the $\nu = 0$ Bessel function basis (see the MATLAB code [12] for $l = 0$ and also Ref. [8] for other possible DVR basis sets in 1D).

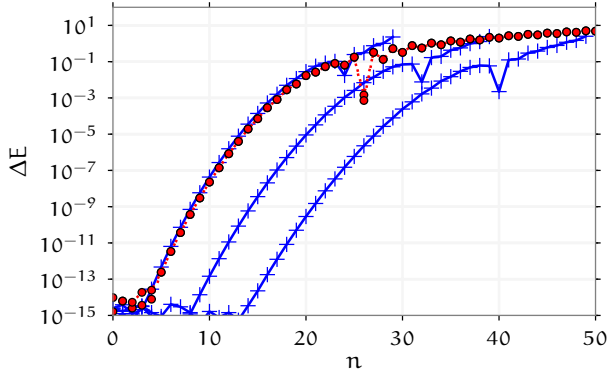


Figure 1. (color online) Difference in spectrum between the DVR Hamiltonian (25) and the HO energies $(n + 1/2)\hbar\omega$. The three (blue) curves with pluses have fixed uv scale (lattice constant $a = 1$, $k_c = \pi/a$) with $L \in \{30, 40, 50\}$ and $\omega = 2\pi/L$ from left to right. The (red) curves with dots have fixed $L = 30$ but varying lattice constant $a \in \{1/2, 1/3\}$ demonstrating the uv convergence. The sizes of the DVR basis sets are $Lk_c/\pi = 30, 40,$ and 50 (blue pluses) and $60,$ and 90 (red circles) respectively. For the blue pluses, the corresponding number of harmonic oscillator wave functions suggested in Refs. [1, 2] (see also Eqs. (4)), would be $N = Lk_c/4 = L\pi/4a \approx 24, 31, 39$ and $47, 71$ respectively. Notice that the size of the DVR basis set can be reduced by factor of 2 to $Lk_c/2\pi = 15, 20, 25$ (blue) and $30, 45$ (red) respectively, by imposing Dirichlet boundary conditions, however, in that case, states not localized to a single cell will not be reproduced.

In Fig. 1 we show the energy differences between the eigenvalues of the Hamiltonian (25) and $\hbar\omega(n + 1/2)$. These “errors” are indicative only of the energy shifts due to the tunneling between neighbouring cells in the case of periodic boundary conditions, as one can judge by comparing systems with different lengths at the same energy, when the tunneling matrix elements are similar. The results for the lowest 2/3 of the spectrum are, for all practical purposes, converged in the DVR method, and the harmonic oscillator basis set is worse in this case. With $N = Lk_c/4 \approx 24$ one can obtain at most 10 states or so with a reasonable accuracy in this reduced interval on the x -axis with periodic or Dirichlet boundary conditions, if one were to follow the prescription of Refs. [1, 2].

In Fig. 2 we demonstrate the uv and IR exponential convergence of the DVR method for an asymmetric short-range potential with analytic wavefunctions. Note that both IR and uv errors scale exponentially until machine precision is achieved – $\Delta E \propto \exp(-2k_\infty L)$ (left) and $\Delta E \propto \exp(-2k_c r_0)$ (right) respectively, where r_0 is potential dependent and k_∞ is determined by the bound state energy $E = -\hbar^2 k_\infty^2 / 2m$. These exponential scalings follow from simple Fourier analysis (uv) and band structure theory (IR) for short-ranged smooth potentials. Note in particular that the linear uv scaling (right) dif-

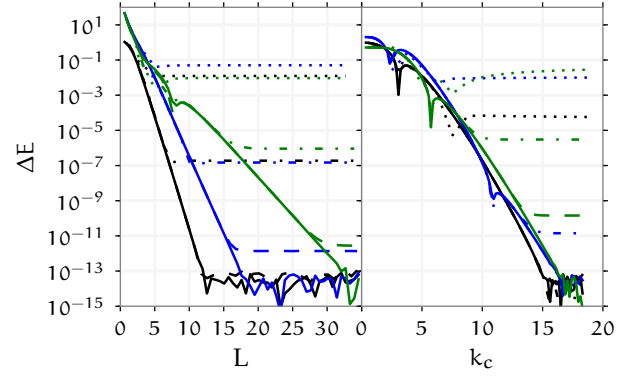


Figure 2. (color online) Here we demonstrate the exponential convergence of the periodic DVR basis for the energy of the bound states of analytically solvable Scarf II potential $V(x) = [a + b \sinh x] / \cosh^2 x$. With $a = 7/2$ and $b = -11/2$, the potential has three bound states – $E_n = -(3 - n)^2/2$ (shown in black, blue, and green from left to right respectively). In the left plot, we demonstrate the IR convergence for increasing L with fixed k_c , while in the right plot we demonstrate the uv convergences for increasing k_c for fixed L . The various values for $k_c \in \{5, 10, 15, 20\}$ (left) and $L \in \{5, 15, 25, 35\}$ (right) correspond to dotted, dot-dashed, dashed, and solid lines with increasing convergence respectively.

fers from the quadratic empirical dependence discussed in [1].

In summary, the DVR basis seems ideal for nuclear structure calculations. It is near optimal in size, and can deliver results with exponential convergence. This DVR basis shares the important advantages of the HO basis set: efficiently separating out the center-of-mass motion using Jacobi coordinates (with the added benefit of not needing to evaluate Talmi-Moshinsky coefficients), utilizing symmetries to reduce the basis size (spherical with the Bessel function DVR), and coverage of the low-energy HO spectrum. Moreover, matrix elements are easy to evaluate – the potential matrix is diagonal for local potentials (no overlap integrals are needed – see for example Eq. (19)), and the kinetic energy matrix is sparse and explicitly expressed analytically. Furthermore, the uv and IR convergence properties of the basis appear on an equal footing, and are clearly expressed in terms of the momentum-space projection and finite box size, allowing for simplified and sound convergence analysis.

We thank G.F. Bertsch for discussions. Ideas described here were developed with support under US DOE grants DE-FG02-97ER41014, DE-FC02-07ER41457, DE-FG02-00ER41132, and DE-FG02-00ER41132.

-
- [1] R. J. Furnstahl, G. Hagen, and T. Papenbrock, Phys. Rev. C **86**, 031301 (2012), arXiv:1207.6100.
- [2] S. A. Coon, M. I. Avetian, M. K. G. Kruse, U. van Kolck, P. Maris, and J. P. Vary, Phys. Rev. C **86**, 054002 (2012), arXiv:1205.3230.
- [3] R. W. Hamming, *Numerical Methods for Scientists and Engineers* (McGraw-Hill, Inc., New York, NY, USA, 1973).
- [4] One of the best numerical implementation of the FFT is *The Fastest Fourier Transform in the West*, www.fftw.org, developed by M. Frigo and S.G. Johnson.
- [5] R. G. Littlejohn and M. Cargo, J. Chem. Phys. **116**, 7350 (2002).
- [6] R. G. Littlejohn, M. Cargo, T. Carrington, Jr., K. A. Mitchell, and B. Poirier, J. Chem. Phys. **116**, 8691 (2002).
- [7] R. G. Littlejohn and M. Cargo, J. Chem. Phys. **117**, 27 (2002).
- [8] D. Baye, physica status solidi (b) **243**, 1095 (2006).
- [9] E. Beth and G. E. Uhlenbeck, Physica **4**, 915 (1937).
- [10] M. Lüscher, Comm. Math. Phys. **104**, 177 (1986).
- [11] N. Nygaard, G. M. Bruun, B. I. Schneider, C. W. Clark, and D. L. Feder, Phys. Rev. A **69**, 053622 (2004), arXiv:cond-mat/0312258.
- [12] On www.phys.washington.edu/~bulgac follow the link *Numerical Programs*. This code implements a fully self-consistent solution using the Bessel-function DVR basis to find the ground state of even and odd numbers of harmonically trapped fermions in the unitary limit, and was used for obtaining the results published in Ref. [15].
- [13] The complete python codes for these plots and related MATLAB codes can be found at https://bitbucket.org/mforbes/paper_dvr_vsho.
- [14] A. Bohr and B. R. Mottelson, *Nuclear Structure* (World Scientific, Singapore, 1998).
- [15] A. Bulgac, Phys. Rev. A **76**, 040502 (2007), arXiv:cond-mat/0703526.